Electronic Supplementary Information

New insights into the dissociation dynamics of methylated anilines

Neil C. Cole-Filipiak[1,2] and Vasilios G. Stavros[1,*]

[1] *Department of Chemistry, University of Warwick, Library Road, Coventry, CV4 7AL, United Kingdom*

[2] *Present address: Combustion Research Facility, Mail Stop 9055, Sandia National Laboratories, Livermore, CA 94551–0969, USA*

[*] Electronic mail: v.stavros@warwick.ac.uk.

S1 Details of the New Ion Detector

Motivated by the accumulation of damage in the centre of our imaging MCP detector, we have installed a new ion detector that is moveable under vacuum. A 25 mm active area MCP with a metal anode detector (Del Mar Photonics MCP-MA25/2) has been mounted on the end of a rotary feedthrough, as shown in Fig. S1. When the plane of the detector is parallel to the ion flight path, ions are shielded from all of the new detector electronics (as well as the feedthrough holes in the magnetic shielding) by the tube protruding out from the third VMI plate. This configuration allows us to image scattered photoproducts as described in the main paper. The new detector may then be rotated 90° into the ion flight path and used to measure intense ion signals without damage to the position-sensitive imaging detector.

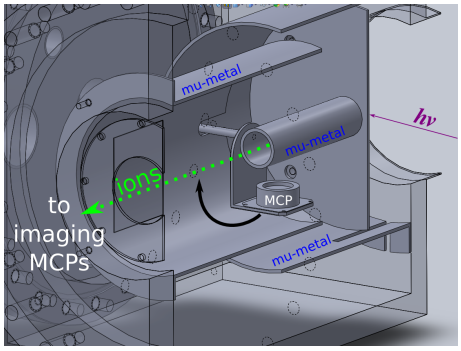

Figure S1: Schematic of the new ion detector.

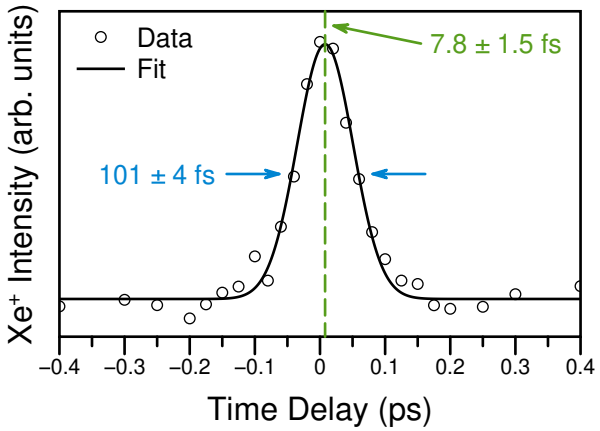

Figure S2: Example Xe^+ transient at $\lambda_{pu} = 245$ nm and $\lambda_{pr} = 243$ nm (black circles) and accompanying Gaussian fit (black line). The FWHM and t_0^{true} are given in the figure.

S2 Details of the Kinetic Model

S2.1 Instrument Response Function and $\Delta t = 0$

The instrument response function (IRF) was taken to be the time resolved ion yield from the non-resonant ionisation of Xe, an example of which is shown in Fig. S2. These transients were fit to a Gaussian function to measure both the maximum temporal overlap $\Delta t = 0$, t_0^{true} in Eq. (S1), and cross-correlation of the two laser pulses. The latter was taken to be the full width at half maximum (FWHM) of the Gaussian fit; 100−120 fs were typical.

S2.2 H-atom Appearance Model

The model used to fit our one-dimensional H^+ transient data assume parallel excited state decay pathways, *i.e.* all dynamics begin at $\Delta t = 0$. Briefly, a sum of exponential rise functions in forward time delay ($\Delta t > 0$), an exponential rise in the probe-initiated "reverse" time delay ($\Delta t < 0$),[1] and one exponential decay in forward and reverse time delay are multiplied by a step function and convoluted with a Gaussian function to model the IRF. The total model is thus:

$$S(t) = S_0 + g(t) * u(t) \cdot \left\{ \sum_n A_n \left[1 - \exp\left(-\frac{t}{\tau_n^{\mathrm{H}}} \right) \right] + B \exp\left(-\frac{t}{\tau_{\mathrm{decay}}} \right) \right\} + g(t) * u(-t) \cdot \left\{ C \left[1 - \exp\left(\frac{t}{\tau_{\mathrm{rev}}^{\mathrm{H}}} \right) \right] + D \exp\left(\frac{t}{\tau_{\mathrm{rev,decay}}} \right) \right\} \quad \text{(S1)}$$

where $t = \Delta t - t_0^{true}$, $S(t)$ is the time delay dependent signal, S_0 is the signal baseline (assumed to be zero for the subtracted transients), $g(t)$ is the Gaussian function, and A–D are the exponential amplitudes. Lifetimes τ_i^{H} are referred to as "appearance lifetimes" as

these terms describe the rise in H^+ signal due to neutral production of H-atoms (*e.g.* by single pump photon photodissociation); the other lifetimes, all associated with exponential decay functions, describe time-dependent dissociative ionisation to produce H^+. The function $u(t)$ is a step function such that:

$$u(t) = \begin{cases} 0 & \text{if } t < 0, \\ 1 & \text{if } t \geq 0. \end{cases}$$

S2.3 Exponential Decay Model

Similar to Eq. (S1), and as mentioned in the main paper, the highest TKER signal was fit using sums of exponential decays:

$$S(t) = S_0 + g(t) * \left[\sum_i A_i \exp\left(-\frac{t}{\tau_i}\right) H(t) + \sum_j A_j \exp\left(\frac{t}{\tau_j}\right) H(-t) \right] \tag{S2}$$

where i and j denote forward and reverse exponential decays, respectively.

S3 Computational Results

Details of the quantum chemical computational methods may be found in the Experimental section of the main paper.

S3.1 Excited States of NMA

Table S1: Excited states of NMA including energies, oscillator strengths, transition composition, and final state assignments based on the dominant transition. The orbitals involved in each transition, reported as H and L for HOMO and LUMO, are shown in Fig. S3.

State	Energy (eV)	Oscillator Strength	Transition	Amplitude	Assignment
1	4.714	0.029	H → L+3	0.740	$^1\pi\pi^*$
			H → L	0.566	
			H−1 → L+7	0.224	
2	4.832	0.018	H → L	0.721	N 3s ($^1\pi\sigma^*$)
			H → L+3	0.542	
			H → L+4	0.227	
3	5.293	0.023	H → L+1	0.870	N 3p
			H → L+7	0.243	
			H → L	0.201	
4	5.451	0.102	H → L+7	0.603	$^1\pi\pi^*$
			H → L+2	0.590	
			H → L+1	0.293	
			H−1 → L+3	0.232	
5	5.500	0.052	H → L+2	0.746	C 3s and 3p
			H → L+7	0.483	
			H → L+6	0.253	

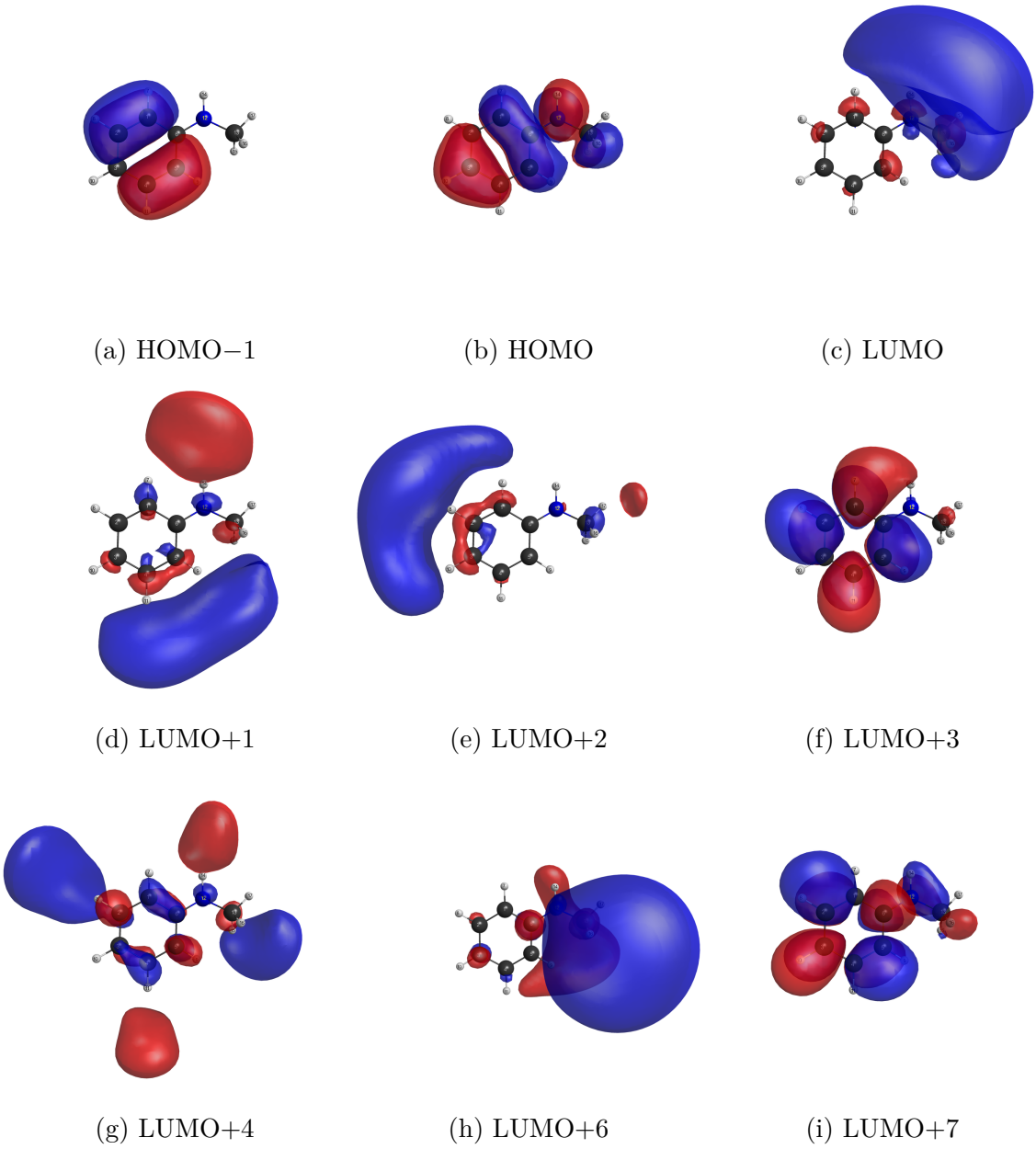

(a) HOMO−1 (b) HOMO (c) LUMO

(d) LUMO+1 (e) LUMO+2 (f) LUMO+3

(g) LUMO+4 (h) LUMO+6 (i) LUMO+7

Figure S3: Molecular orbitals involved in the first five excited states of NMA shown in Table S1. The HOMO and HOMO−1 orbitals are of π character, the LUMO+3 and LUMO+7 orbitals are of π^* character, and the remaining LUMO orbitals are of N or C centred Rydberg orbitals.

S3.2 Calculated β_{H} Parameter

An experimental β_{H} parameter may be estimated from the calculated geometries of NMA using the equation:

$$\begin{aligned}\beta_{\mathrm{H}} &= 2\mathrm{P}_2(\cos\chi) \\ &= 3\cos^2\chi - 1 \end{aligned} \tag{S3}$$

where $\mathrm{P}_2(x)$ is the second order Legendre polynomial and χ is the angle between the excited state transition dipole moment and the dissociating bond (*i.e.* the N–H bond).[2] Assuming that NMA remains at the Franck-Condon geometry, the β_{H} parameters for the first five excited states may be calculated using the atom coordinates and transition dipole moments listed in Table S2 by substituting the following into Eq. (S3):

$$\cos\chi = \frac{\mathbf{v}_{\text{N–H}} \cdot \mathbf{v}_{\text{TDM}}}{||\mathbf{v}_{\text{N–H}}||\,||\mathbf{v}_{\text{TDM}}||}$$

$$\text{where} \quad \mathbf{v}_{\text{N–H}} = \begin{pmatrix} x_{\mathrm{N}} - x_{\mathrm{H}} \\ y_{\mathrm{N}} - y_{\mathrm{H}} \\ z_{\mathrm{N}} - z_{\mathrm{H}} \end{pmatrix} \quad \text{and} \quad \mathbf{v}_{\text{TDM}} = \begin{pmatrix} x_{\text{TDM}} - 0 \\ y_{\text{TDM}} - 0 \\ z_{\text{TDM}} - 0 \end{pmatrix}.$$

The resulting $\beta_{\mathrm{H}}^{\text{calc}}$ values reveal that excitation to State 3 ($^1\pi$3p) or State 4 ($2^1\pi\pi^*$) most closely reproduces the experimental $\beta_{\mathrm{H}} \approx -0.3$.

Table S2: Cartesian coordinates (Å) for the ground state N–H geometry and transition dipole moments for the first five excited states of NMA listed in Table S1.

Atom or Vector	x	y	z	$\beta_{\mathrm{H}}^{\text{calc}}$
N12, S_0 geometry	1.8326	0.5817	−0.1243	—
H14, S_0 geometry	2.0584	1.5199	0.1677	—
State 1 TDM	0.3354	−0.8812	−0.0671	0.96
State 2 TDM	−0.4197	0.6058	−0.0376	0.16
State 3 TDM	0.7447	0.0909	0.2561	−0.49
State 4 TDM	−1.6323	−0.2079	−0.1175	−0.61
State 5 TDM	1.0630	0.2103	−0.4388	−0.79

S3.3 Geometry of the D_0^+ State

While the amine of NMA is pyramidal in the S_0 state, the ground cationic state is planar; thus probe ionisation of the neutral molecule (particularly in the Franck-Condon region near $\Delta t = 0$) will result in a vibrationally excited cation. This vibrational excitation will be diminished or non-existent for Rydberg states whose "atomic-like" orbitals have a reduced dependence upon molecular geometry. To aid the interpretation of the TR-PES spectra, the energies and harmonic frequencies of the NMA D_0^+ state were calculated at the S_0 (*i.e.* the Franck-Condon geometry) and D_0^+ equilibrium geometries, yielding a zero-point energy corrected difference of 2165 cm^{-1}. Thus, in the Franck-Condon region near $\Delta t = 0$, ionisation of NMA valence orbitals will result in ∼2000 cm^{-1} of vibrational excitation in the D_0^+ state.

S4 Additional Results

Table S3: TR-PES decay lifetimes for NMA, 3,5-DMA, and *N,N*-DMA assuming parallel dynamics at the pump wavelengths indicated; errors reported are the standard error of the fit.

Molecule, λ_{pu} (nm)	τ_1 **(fs)**	τ_2 **(fs)**	τ_3 **(ps)**	τ_4 **(ps)**	τ_5 **(ns)**
NMA, 238	< 50	141 ± 5	1.3 ± 0.1	68.0 ± 1.4	> 0.5
NMA, 245	< 50	136 ± 7	0.80 ± 0.05	131 ± 4	> 1.2
3,5-DMA, 238	< 50	82 ± 4	1.05 ± 0.07	127 ± 2	> 1.2
N,N-DMA, 238	< 50	81 ± 2	1.074 ± 0.008	140 ± 20	0.88 ± 0.08

S4.1 *N*-methylaniline

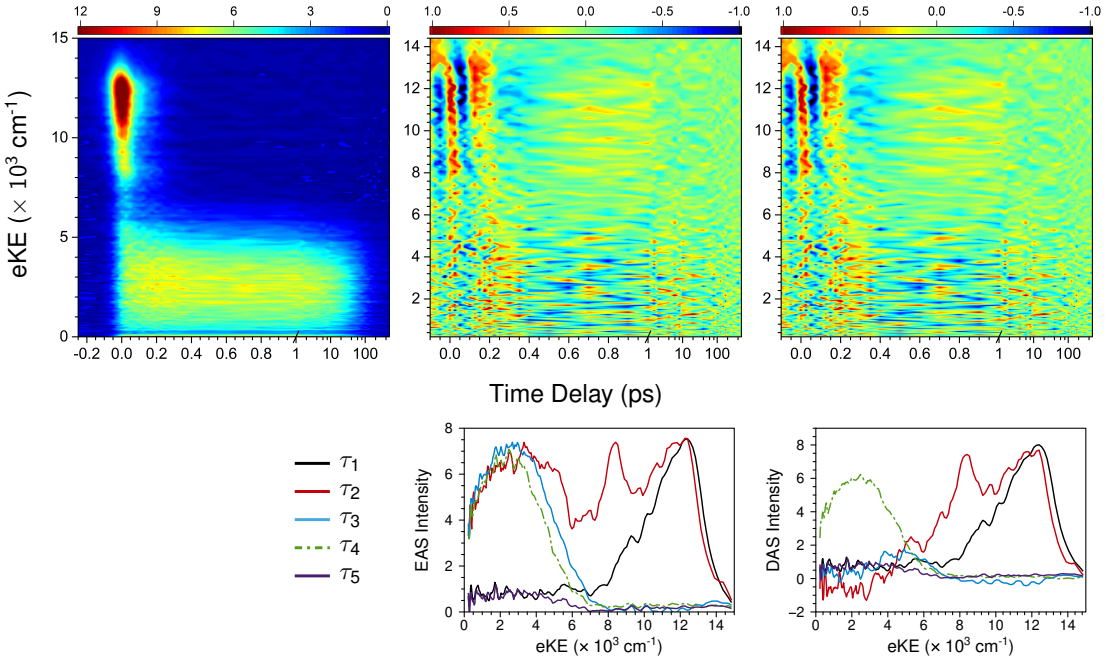

Figure S4: TR-PES results from NMA at $\lambda_{pu} = 238$ nm and $\lambda_{pr} = 305$ nm (left). Also shown are the fit residuals for sequential (middle) and parallel (right) model fits with corresponding EAS and DAS shown below. DAS time constants are shown in Table S3. The EAS and DAS have been smoothed using a 3 point moving average; the τ_1 DAS and EAS have been scaled for visual clarity. The negative τ_2 DAS intensity below 4000 cm^{-1} is indicative of sequential population transfer from either the $2^1\pi\pi^*$ or $^1\pi$3s state onto the $1^1\pi\pi^*$ state.

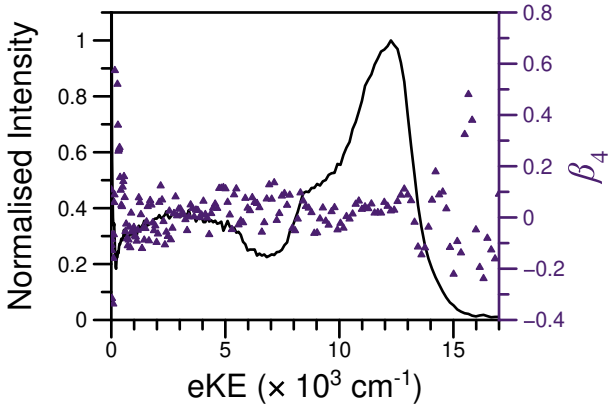

Figure S5: Photoelectron and β_4 spectra for NMA at $\lambda_{pu} = 238$ nm near $\Delta t = 0$. An average value of $\beta_4 \approx 0$ is evident across the entire spectrum. While it is tempting to attribute the apparent dip at ∼13 000 cm^{-1} to a Rydberg state, the large β_4 oscillations at higher eKE (likely arising from the near-zero TR-PES intensity) would cast significant doubt on such an assignment.

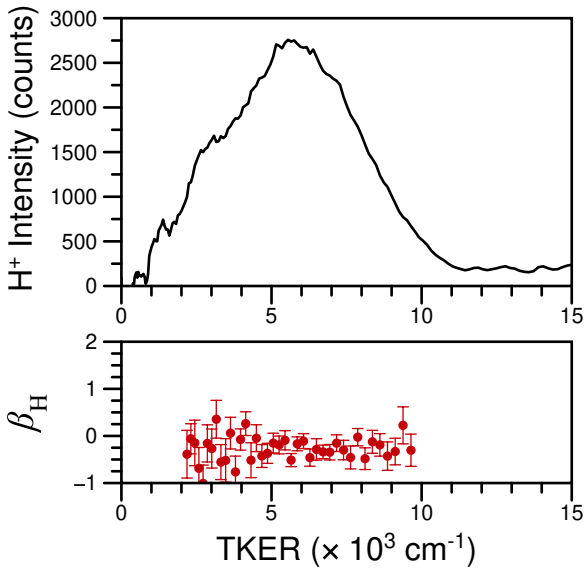

Figure S6: Example H$^+$ TKER (top) and β_H (bottom) spectra for NMA at $\lambda_{pu} = 238$ nm and $\Delta t = 100$ ps.Error bars are computed during POP deconvolution and correspond to one standard deviation of the difference between the fit and experimental angular distributions at each KE. Every other β_H point has been omitted for visual clarity.An average value of $\beta_H \approx -0.3$ is evident across the entire TKER feature. The TKER spectrum has been smoothed using a 10 point moving average.

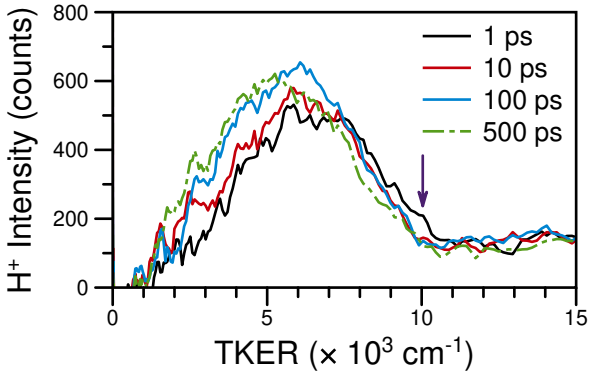

Figure S7: Example NMA H^+ TKER spectrum at $\lambda_{pu} = 252$ nm and $\Delta t = 1$ ps (black line), 10 ps (red line), 100 ps (blue line), and 500 ps (green, dash-dot line); spectra have been smoothed using a 20 point moving average. The $TKER_{max}$ is shown as a purple arrow.[3] The slight rise in signal at low TKER and $\Delta t = 100$ and 500 ps may indicate that a second H-atom loss mechanism, similar to the one discussed in the main paper, may be accessible when photoexciting the $1^1\pi\sigma^*$ or $1^1\pi\pi^*$ state of NMA; further investigation would be of interest.

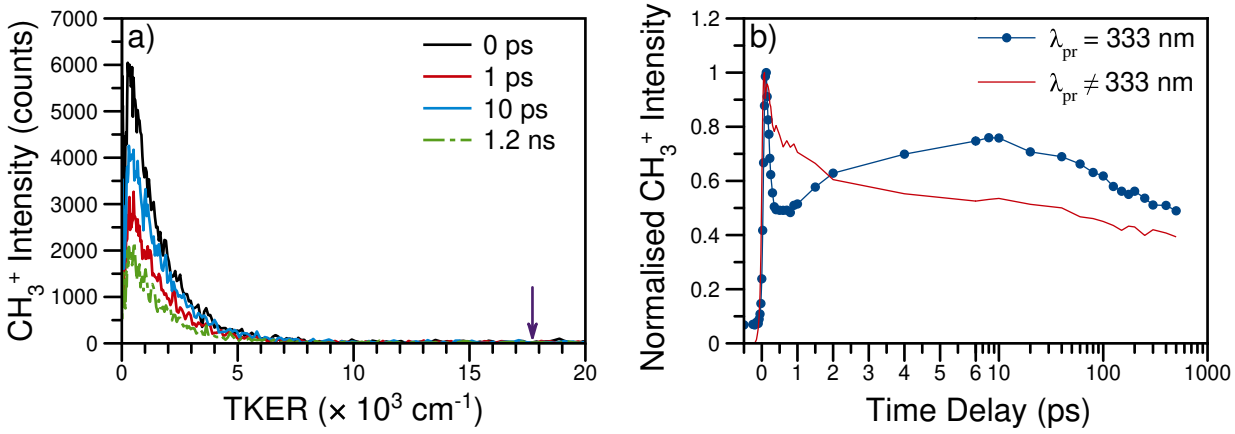

Figure S8: a) Example NMA CH_3^+ TKER spectra at $\lambda_{pu} = 238$ nm and $\lambda_{pr} = 333$ nm. The expected $TKER_{max}$ is shown as a purple arrow.[3] b) CH_3^+ transients at the same pump wavelength; "on resonance" λ_{pr} data are shown as connected, blue circles while the non-resonant λ_{pr} are shown as a solid red line. The rise observed near $\Delta t = 10$ ps is due to multiphoton pump photoexcitation, likely populating a cationic state which dissociates to produce neutral CH_3.

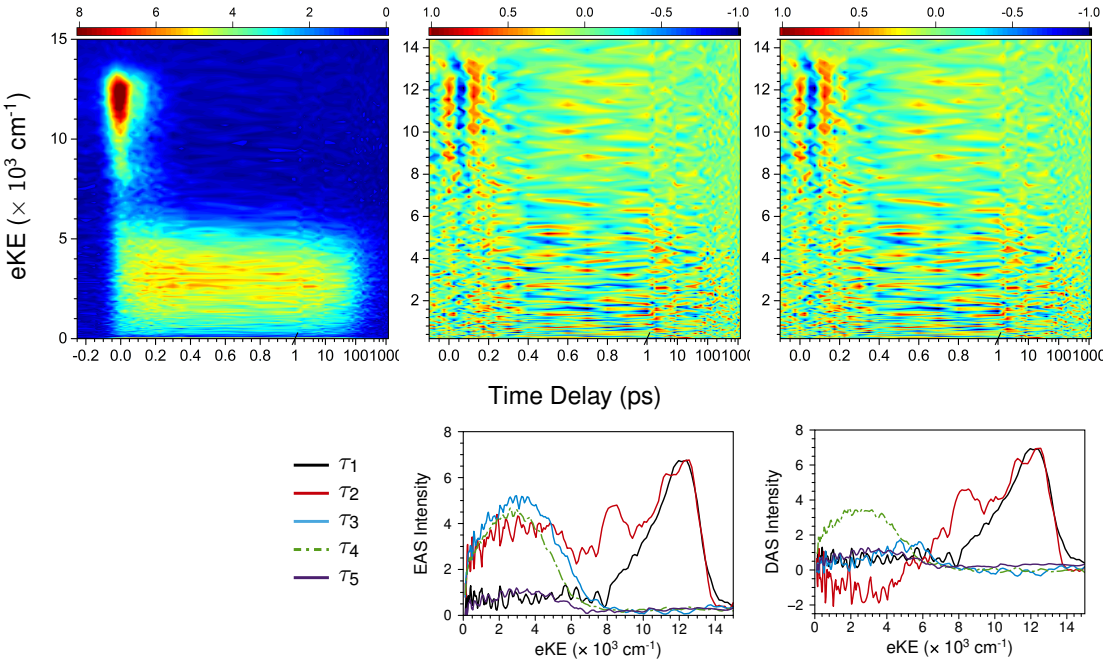

Figure S9: TR-PES results from NMA at $\lambda_{pu} = 245$ nm and $\lambda_{pr} = 305$ nm (left). Also shown are the fit residuals for sequential (middle) and parallel (right) model fits with corresponding EAS and DAS shown below. DAS time constants are shown in Table S3. The EAS and DAS have been smoothed using a 3 point moving average; the τ_1 DAS and EAS have been scaled for visual clarity. The negative τ_2 DAS intensity below 5000 cm^{-1} is indicative of sequential population transfer from either the $2^1\pi\pi^*$ or $^1\pi 3s$ state onto the $1^1\pi\pi^*$ state.

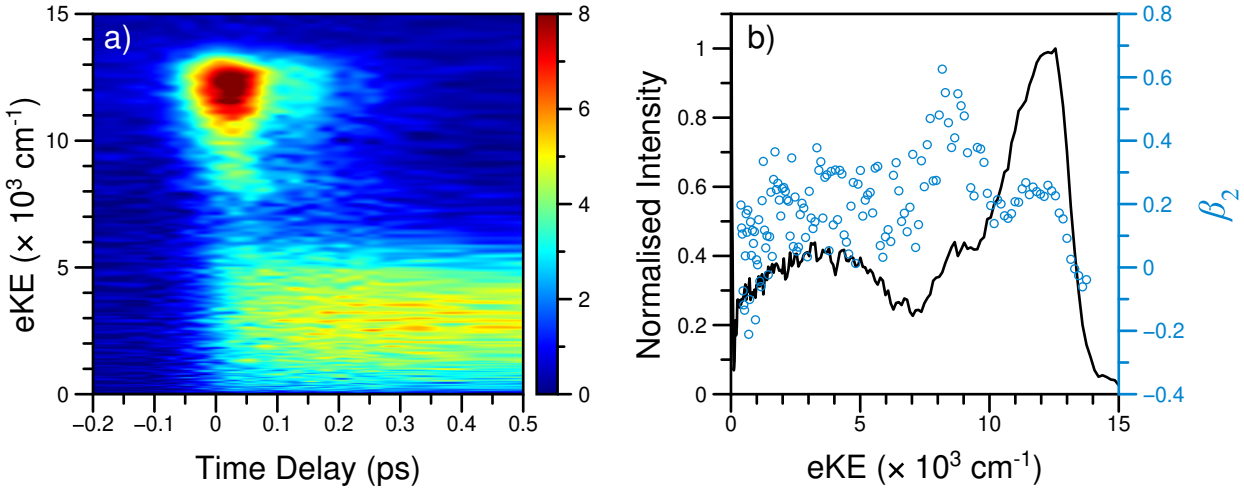

Figure S10: a) Short time delay TR-PES results from NMA at $\lambda_{pu} = 245$ nm and $\lambda_{pr} = 305$ nm. b) The PES (black line) and β_2 distribution as a function of eKE (blue circles) near $\Delta t = 0$.

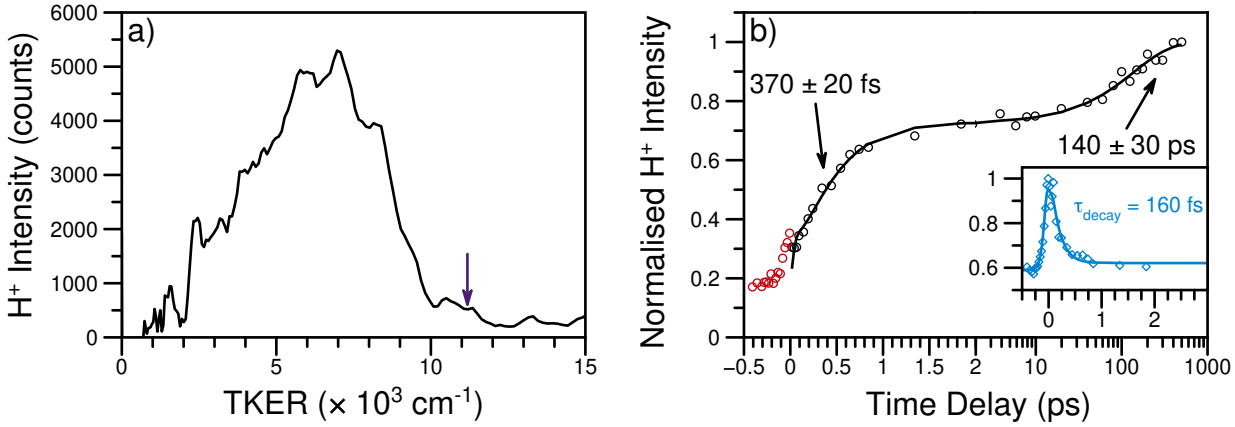

Figure S11: a) Example NMA H^+ TKER spectrum at $\lambda_{pu} = 245$ nm and $\Delta t = 2$ ps the spectrum has been smoothed using a 5 point moving average. The $TKER_{max}$ is shown as a purple arrow.[3] b) H^+ transient again revealing two rises in H^+ intensity; appearance lifetimes are given in the figure and in Table 1 of the main paper. Inset: H^+ transient from TKER > 11 000 cm^{-1}. The exponential decay lifetime from this region (τ_{decay}) was included in the fit at lower TKER to account for the time-dependent, non-resonant production of H^+; see Eq. (S1) for further details.

S4.2 Aniline, 3,5-DMA, and *N*,*N*-DMA

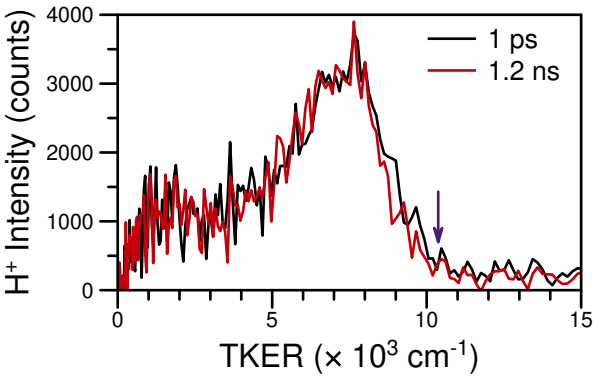

Figure S12: Example aniline TKER spectra at $\lambda_{pu} = 238$ nm. The $TKER_{max}$ is shown as a purple arrow.[4] As implied by a previous investigation,[5] aniline has only one ultrafast (*i.e.* within 1.2 ns) H-atom loss mechanism.

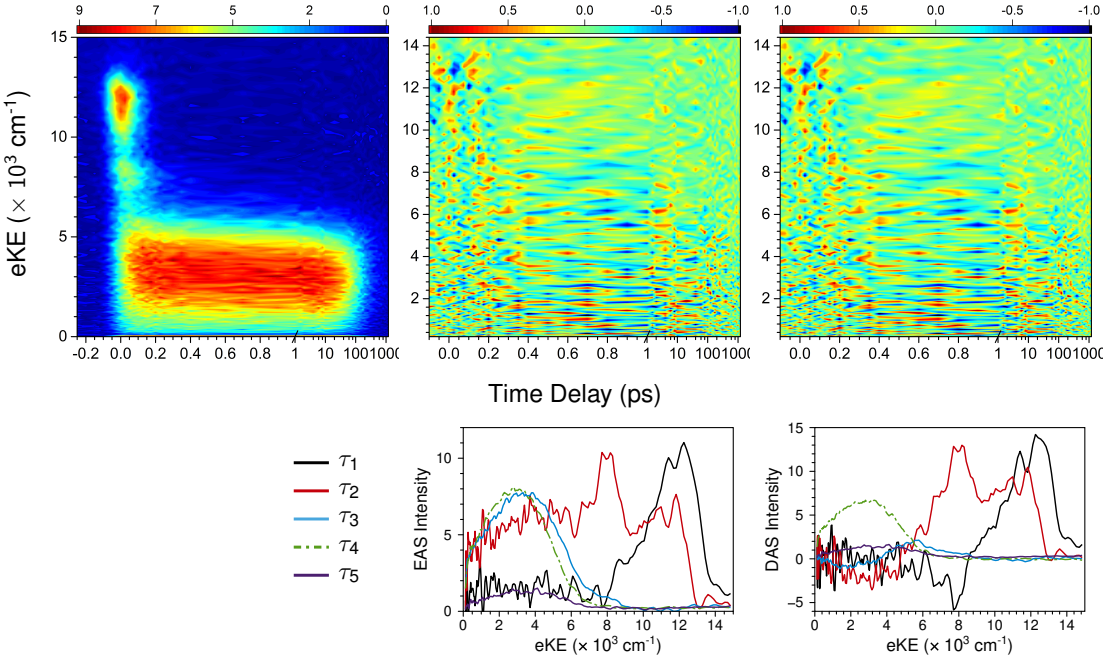

Figure S13: TR-PES results from 3,5-DMA at λ_{pu} = 238 nm and λ_{pr} = 305 nm (left). Also shown are the fit residuals for sequential (middle) and parallel (right) model fits with corresponding EAS and DAS shown below. DAS time constants are shown in Table S3. The EAS and DAS have been smoothed using a 3 point moving average; the τ_1 DAS and EAS have been scaled for visual clarity. The negative τ_1 DAS intensity around 8000 cm^{-1} indicates sequential population transfer from the $2^1\pi\pi^*$ state onto the $^1\pi$3s state. Similarly, the τ_2 DAS intensity below 5000 cm^{-1} suggests sequential population transfer from either the $2^1\pi\pi^*$ or $^1\pi$3s state onto the $1^1\pi\pi^*$ state.

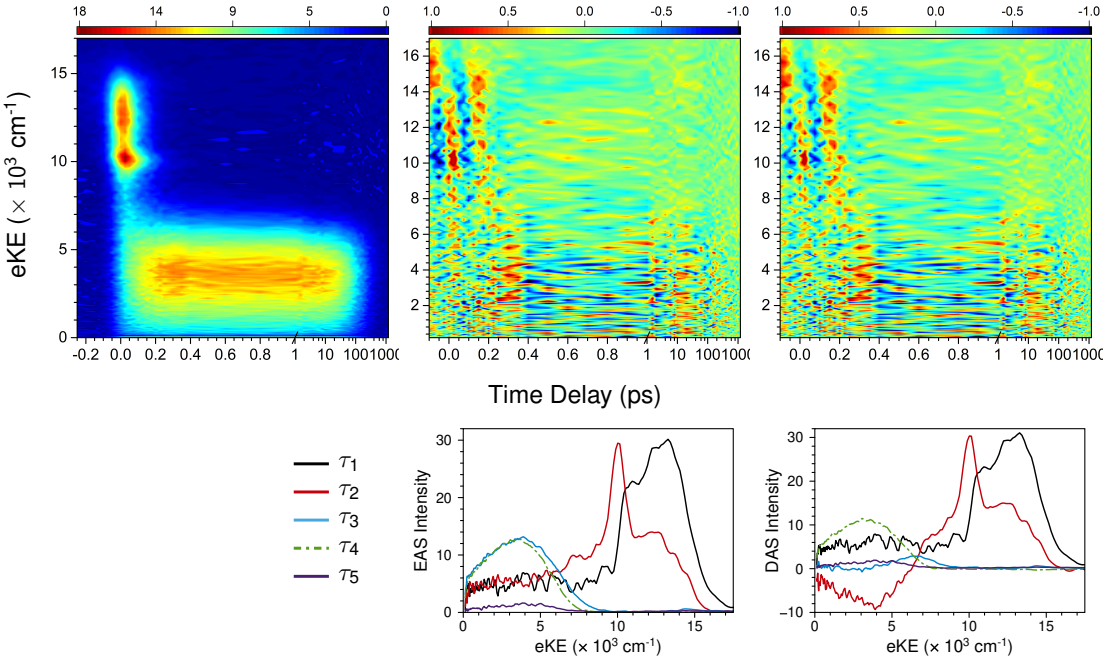

Figure S14: TR-PES results from *N,N*-DMA at $\lambda_{pu} = 238$ nm and $\lambda_{pr} = 305$ nm (left). Also shown are the fit residuals for sequential (middle) and parallel (right) model fits with corresponding EAS and DAS shown below. DAS time constants are shown in Table S3. The EAS and DAS have been smoothed using a 3 point moving average; the τ_1 DAS and EAS have been scaled for visual clarity. The negative τ_2 DAS intensity below 4000 cm^{-1} is indicative of sequential population transfer from either the $2^1\pi\pi^*$ or $^1\pi$3s state onto the $1^1\pi\pi^*$ state.

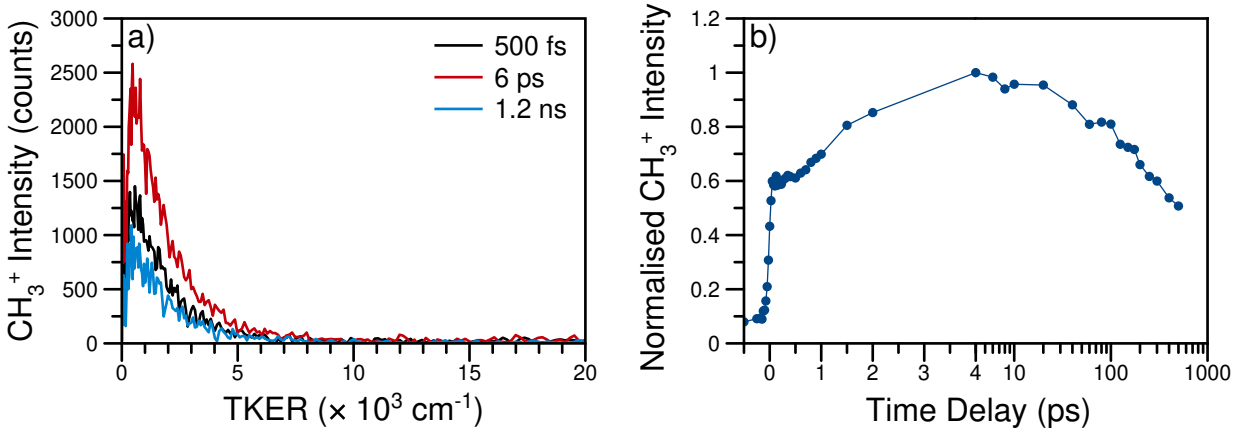

Figure S15: a) Example *N,N*-DMA CH_3^+ TKER spectra at $\lambda_{pu} = 238$ nm. b) CH_3^+ transient at the same pump wavelength; data are shown as connected, blue circles.While the rise in CH_3^+ signal near $\Delta t = 4$ ps appears to be due to single pump photoexcitation, the probe pulse may still provide enough energy to sample a dissociative cationic surface. However, given the similarity between the TKER spectra and transient to the NMA results shown in Fig. S8, a $m/z = 15$ transient was not recorded with an off-resonant probe for *N,N*-DMA.

S5 Details of the Zenodo Archive

Data underpinning the present results are freely available through the Zenodo data repository at doi:10.5281/zenodo.1488380. All data are saved as a `.csv` file. Each transient `.csv` file is labeled according to molecule, pump wavelength, data type, and a date (*e.g.* `NMA_238_TRPES_11Oct2017.csv`). The first column contains kinetic energies (either eKE or TKER) while the first row indexes each time delay. The normalised UV absorption spectra are saved in one file, with columns for each molecule.

References

[1] H. Lippert, H.-H. Ritze, I. V. Hertel, and W. Radloff, ChemPhysChem **5**, 1423 (2004).

[2] H. Kim, K. S. Dooley, S. W. North, G. E. Hall, and P. L. Houston, J. Chem. Phys. **125**, 133316 (2006).

[3] A. J. Colussi and S. W. Benson, Int. J. Chem. Kinet. **10**, 1139.

[4] G. A. King, T. A. A. Oliver, and M. N. R. Ashfold, J. Chem. Phys. **132**, 214307 (2010).

[5] G. M. Roberts, C. A. Williams, J. D. Young, S. Ullrich, M. J. Paterson, and V. G. Stavros, J. Am. Chem. Soc. **134**, 12578 (2012).